Nanoscale

PAPER

View Article Online
View Journal | View Issue

Cite this: *Nanoscale*, 2023, **15**, 6984

Modifying flexible polymer films towards superhydrophobicity and superoleophobicity by utilizing water-based nanohybrid coatings†‡

Fanourios Krasanakis,[a] Thaleia-Michaela Chatzaki,[a,b] Kiriaki Chrissopoulou *[a] and Spiros H. Anastasiadis *[a,b]

The development of superhydrophobic and/or superoleophobic materials has been attracting the attention of the scientific community due to their wide range of applications. In this work, waterborne nanocomposite coatings were developed to be deposited onto flexible polyethylene films in order to modify them into superhydrophobic and even superoleophobic. The coatings consisted of either a low surface energy mixture of silanes/siloxanes or a fluoropolymer in conjunction with the appropriate inorganic nanoparticles that provide the necessary roughness; the effects of nanoparticle type and content on the behaviour was investigated. In both cases, the surface properties were investigated, and the polymer films were found to be superhydrophobic. Depending on the system utilized, the final material exhibited either low water adhesion, thus, being water repellent, or high water adhesion. The use of the fluoropolymer has led to coatings that exhibited superoleophobic behaviour for various organic compounds, as well. The application of the coatings did not influence either the optical transparency or the thermal properties of the polyethylene films. Moreover, the coated surfaces show similar or even better mechanical properties, scratch resistance and chemical durability in comparison to the neat LDPE film.

Received 4th December 2022,
Accepted 2nd March 2023

DOI: 10.1039/d2nr06780c

rsc.li/nanoscale

1. Introduction

The interest in superhydrophobic surfaces has grown significantly over recent decades due to their wide range of applications as well as their importance in fundamental research.[1,2] Self-cleaning surfaces,[3–5] anti-fouling[6–8] and self-healing materials,[9,10] stain resistant textiles[11–13] or anti-icing coatings[14,15] are examples that demonstrate the significant potential of such materials. Surfaces can be classified as superhydrophobic and water repellent when the contact angle of a water droplet is higher than ~150° and the contact angle hysteresis is less than[16,17] ~10° or as superhydrophobic with high water adhesion, when the water contact angles are similarly high but the contact angle hysteresis is high as well.[18,19] The main strategy employed for the development of superhydrophobic materials is mimicking superhydrophobic biosurfaces in nature by exploring various surface compositions and structures observed in different plants and/or insects.[20] One of the most famous examples of superhydrophobic and water repellent surfaces in nature is the sacred Lotus leaf (*Nelumbo nucifera*);[21,22] its behaviour is attributed to the dual-scale hierarchical roughness created by the papillose epidermal cells of the leaf (at the ~5–10 micrometer length scale) combined with the additional layer of hydrophobic epicuticular waxes (at the ~100 nm length scale).[23] The superhydrophobic and water repellent character leads to self-cleaning surfaces, where the water droplets can roll off the surface of the leaf, thus, removing any dust particles. Similar behaviour is observed in other plants as well, like taro or rice leaves.[24] Moreover, shark skin, duck feathers, gecko feet and the wings of insects are other examples in animal life, which exhibit highly hydrophobic properties, whereas the corrugated surfaces on the duck feet entrap air pockets, which prevent the adhesion of water.[25] At the same time, the presence of superhydrophobic surfaces on insects leads to prevention of water (and weight) accumulation and bacterial growth, to low adhesion of foreign particles, as well as to the rolling of water droplets, which entrain and remove any contaminants stuck onto the surface.[26,27] It is, thus, generally understood that it is the hierarchical roughness of the micro/nano-structured surface in conjunction with the appropriate hydrophobic chemical composition that control the behaviour.[28–32]

[a]*Institute of Electronic Structure and Laser, Foundation for Research and Technology-Hellas, 711 10 Heraklion, Crete, Greece. E-mail: spiros@iesl.forth.gr, kiki@iesl.forth.gr*
[b]*Department of Chemistry, University of Crete, 710 03 Heraklion, Crete, Greece*
†Dedicated to Professor Thomas P. Russell on the occasion of his 70th birthday.
‡Electronic supplementary information (ESI) available. See DOI: https://doi.org/10.1039/d2nr06780c

There are many chemical and physical methodologies utilized to fabricate superhydrophobic surfaces;[33] these are usually categorized into two types, the top-down and the bottom-up approaches, whereas their combination is frequently used as well.[34,35] Among the most common techniques are the templating method and lithography, which are top-down methods that result in superhydrophobic surfaces with controlled morphology.[36–42] Chemical or plasma etching as well as laser irradiation can develop surfaces with either random or periodic roughness whereas further chemical modification can lead to the desired behaviour.[43–47] Among the bottom-up approaches, the most feasible in industry are dipping,[48,49] spraying[50,51] or spin coating,[52,53] which are very simple and low cost physical deposition techniques. Depending on the conditions (temperature, solvent evaporation rate, solution concentration), these methods can lead to the fabrication of thin films of organic materials even on heterogeneous surfaces.[48]

Much like superhydrophobic surfaces, superoleophobic surfaces have attracted the interest of the scientific community also because of their multiple applications that include the fabrication of corrosion resistant surfaces,[54] the oil/water separation,[55,56] and the prevention of water pipe blockage by oily impurities.[57] However, the fabrication of superoleophobic surfaces in air is much more challenging than that of superhydrophobic surfaces because of the much lower surface tension of oils and organic liquids compared to water.[58]

In cases when a surface coating is to be utilized, one can introduce roughness, and even hierarchical roughness, on a substrate by utilizing various nanoparticles, *e.g.*, silica or metal oxides.[59] The substrates often used are metals, textiles, fabrics, paper, wood surfaces and even stone monuments.[60–68] In all cases, the presence of the nanoparticles enhances the roughness in the nanoscale, which together with the usually inherent roughness in the micron scale can amplify the effects of a hydrophobic chemistry to superhydrophobicity and, even, water repellence. The type of nanoparticles utilized depends on the desired properties of the surface. Zinc oxide nanoparticles are used for extra antibacterial and UV protection in textiles and cotton fabrics.[69–71] Similar properties can be obtained by the presence of TiO_2 nanoparticles,[72,73] because of their photocatalytic ability.[74] Silver nanoparticles can transform a surface not only to superhydrophobic[75] but also to oil repellent.[62] Copper can be used for its antibacterial properties[76] and coatings with alumina particles can be repellent to hot water.[77] Silica, *i.e.*, silicon dioxide nanoparticles, SiO_2, are widely used for water repellent and superhydrophobic coatings *via* low cost dipping or spraying methods.[78,79] They are usually mixed with low surface energy materials such as siloxane emulsions[80] or fluorine based macromolecules[81] and hydrophobic polymers like polystyrene.[82] Nanohybrid coatings containing silica nanoparticles can be used in solar cells and greenhouses because of their high transmittance in combination with their self-cleaning ability.[83,84] Most of the works that utilized inorganic nanoparticles to modify surface properties aimed at enhancing the hydrophobicity of hard solid surfaces and not flexible polymeric films, like, for example, the ones of greenhouse films. It is noted that in the case of flexible textiles, the materials to be modified exhibit a significant inherent roughness and are not as smooth as a polymeric film.

In this work, we report the fabrication of superhydrophobic and superoleophobic polyethylene flexible surfaces *via* an easy, "industrially friendly" method. Waterborne nanohybrid dispersions containing a low surface energy polymer and inorganic nanoparticles were utilized to form a coating onto the polymer film surface by the dipping method and the surface properties of the final film were investigated. Depending on the macromolecular chemistry and the size and concentration of the nanoparticles, surfaces with contact angles ranging from 100° to higher than 150° are developed. Contact angle hysteresis measurements revealed that, depending on the chemistry of the additive, surfaces can be developed with very low contact angle hysteresis, *i.e.*, water repellent with small roll off angles, or with high hysteresis, *i.e.*, with high water adhesion. Moreover, experiments with organic solvents revealed that the coated substrates exhibit oleophobic or even superoleophobic behaviour. Finally, the films were investigated for their optical, thermal and mechanical properties and their chemical resistance. It was shown that the presence of the coating does not affect the optical and thermal properties with the transmittance being very similar to that of the initial polymer film. Moreover, the coated surfaces show similar or even better mechanical properties, scratch resistance and chemical durability in comparison to the neat LDPE film. This fabrication method can be directly introduced in the production line of LDPE films to provide superhydrophobic and superoleophobic properties with self-cleaning ability.

2. Experimental

2.1. Materials

Low density polyethylene, LDPE, films produced by melt blowing for use in greenhouses were received from Plastika Kritis S. A., Heraklion Crete, Greece. The polymer used was ALCUDIA 2203F with a melt flow index 0.3 g per 10 min (190 °C, 2.16 kg) and a density 922 kg m^{-3}. The films were used either right after their production by film blowing or after they underwent corona treatment in order to increase their surface energy, thus, affecting their wettability and the adhesion of the extra coating.

Two different low surface energy materials were utilized for the development of the coatings. One was a waterborne emulsion of silanes and siloxanes with the commercial name Silres BS 4004 (50 wt% in water) from Wacker Chemie AG. The other was a fluoroalkyl silanol in aqueous solution, with the commercial name Dynasylan SIVO 121 (2 wt% in water) from Evonik Industries AG. Moreover, two different kinds of inorganic nanoparticles were used, silicon dioxide (SiO_2) and aluminum oxide (Al_2O_3), which were received and utilized in the form of 40 wt% aqueous dispersions. The SiO_2 (Snowtex ZL) nanoparticles with a radius of R = 67 nm (according to

Dynamic Light Scattering and Transmission Electron Microscopy measurements[85]) were obtained from Nissan Chemical Industries LTD. The Al_2O_3 nanoparticles (PG003), with a radius of R = 75 nm, were obtained from Cabot Corporation. It is noted that the solution of Dynasylan SIVO 121 exhibits an acidic pH (pH ~ 4) and this is why this solution is mixed with the dispersion of the PG003 alumina nanoparticles, which forms a good dispersion at an acidic pH (pH ~ 4–5), as well. Utilization of nanoparticles in neutral or basic pH (like Snowtex ZL), instead of the alumina ones, would have led to their precipitation in the dispersion, rendering it unsuitable for use by the dipping method.

The coatings were prepared *via* a simple mixing of the nanoparticle dispersions with the respective dispersion or solution of the Silres or Dynasylan low surface energy materials, respectively. The deposition of the coatings on the LDPE substrates was performed *via* dipping. A small piece of the LDPE film (4 cm × 1.5 cm) was immersed vertically in the coating dispersion for 20 seconds and was subsequently placed under vacuum overnight. Annealing of the coated films was carried out under vacuum at 60 °C. The anticipated mechanism of interaction of the components of the coating and the LDPE film is as follows: both Silres and Dynasylan possess –SiOH groups that can react, *via* condensation reactions, with functional groups on the surface of the LDPE substrate, which were formed during the corona treatment, resulting in chemical bonding to the substrate. Moreover, condensation reactions can simultaneously take place between the –SiOH groups of Silres BS4004 and the –OH groups on the surface of the SiO_2 nanoparticles leading to the formation of a hydrophobic silicone film chemically bonded to the silica nanoparticles. In the case of Dynasylan, such condensation reactions can lead to the formation of a fluoropolymer also chemically bonded with the LDPE surface and the alumina nanoparticles.

2.2. Characterization

Contact angle measurements. Investigation of the surface properties of the initial, the corona treated and the coated LDPE films was performed with an OCA-35 contact angle measuring device from Dataphysics, with a SCA-20 software. The contact angle measurements were performed with the sessile drop method (static contact angle) and the volume of the drops used were usually 4 μL (rate 0.5 μL s^{-1}). Furthermore, contact angle hysteresis measurements were carried out by the tilting method, where the advancing and receding angles were measured just before the drop begins to move on the tilted substrate. In such measurement, the angle at which the drop moves provides the roll off angle of the surface for the particular drop volume. During the measurement, the substrate was tilted from 0° to 90° at a constant rate of 1° s^{-1} whereas drop volumes between 4 μL to 35 μL were used. For the hydrophobicity measurements, nanopure water was used utilizing a Hamilton 500 mL syringe and, for the oleophobicity measurements, the organic solvents used were glycerol, 1,2-ethylene glycol and dimethylsulfoxide (DMSO) using a manual syringe of 1 mL.

Scanning electron microscopy (SEM). The surface morphology of the original LDPE and of the coated films was imaged by a JOEL, JSM-7000F, field emission scanning electron microscope (FE-SEM). The microscope used has a high resolution of 1.2 nm at 30 kV, with an accelerating voltage from 0.5 to 30 kV and high focal depth (×10 up to 500.00). The magnification of the images for the samples was ×20.000 for 15 kV accelerating voltage.

Attenuated total reflectance-fourier transform infrared spectroscopy (ATR-FTIR). An IRAffinity-1S compact spectrophotometer with a DLATGS detector in combination with a single reflection diamond ATR accessory QATR10 by Shimadzu was utilized for the spectroscopic characterization of the films. All samples were measured in the wavevector range between 400–4000 cm^{-1}, with a resolution of 4 cm^{-1} and all measurements were performed at ambient temperature. For background correction purposes, the corresponding spectra of the empty chamber were recorded for each temperature whereas special care was given so that no bands associated with CO_2 or H_2O were present after the background correction.

Mechanical properties. An Instron 3365 dual column Universal Testing System having an extensiometer was utilized to investigate the mechanical properties of all films. The film specimens had a width of 10 mm. The crosshead speed was set at 500 mm min^{-1} in accordance with EN ISO 527-3:1996

Abrasion tests. The scratch resistance of the films was evaluated *via* a sand paper abrasion test. An aluminium oxide sandpaper of 2000 mesh was chosen as the abrasion surface and each film, having a weight of 100 g on it, was faced down to the sandpaper and moved for 10 cm. The above process was defined as 1 cycle of abrasion whereas overall more than 40 cycles were performed for each tested surface.

Differential scanning calorimetry (DSC). The thermal transitions of the LDPE substrates before and after the deposition of the nanohybrid coatings were measured utilizing a Discovery DSC250 calorimeter (TA Instruments). The experiments were carried out in a range of temperatures from −100 °C to 200 °C with a heating/cooling rate of 10 °C min^{-1} under inert nitrogen flow to prevent the decomposition of the materials.

Light transmission. The effect of the coatings on the transmittance of the polymer substrates was investigated using a Perkin-Elmer Lambda 45 UV/Vis spectrophotometer in a wavelength range from 400 nm to 1000 nm.

X-ray photoelectron spectroscopy (XPS). All measurements were performed using a SPECS, FlexMod XPS spectrometer equipped with a Mg/Al XR-50 dual anode X-ray Source and a 1D-DLD Specs Phoibos analyzer. The XPS survey and high-energy resolution spectra were collected using MgKα radiation (1253.6 eV) and a Flood Gun FG 22/35 electron beam gun (due to the low conductivity of the samples). The pressure in the chamber was in the range of 10^{-9} mbar. The elemental composition given as an atomic percentage (at %) was determined from the XPS spectra using SpecsLabProdigy software.

3. Results and discussion

3.1. Characterization of LDPE substrates

The neat LDPE films were characterized to define their initial surface properties. Fig. 1 shows representative water drops deposited on different positions of the neat LDPE films. Analysis of the drop profiles provides a water contact angle of 97 ± 3° in agreement with values reported in the literature.[86] This value ranks the LDPE surfaces as slightly hydrophobic.

Contact angle hysteresis measurements were carried out to determine the angle at which the water drops roll off the surface. They were performed for different volumes of the water drops, *i.e.*, drops of 4, 10, 20 and 30 μL volume were utilized. Fig. 2 shows snapshots of the water drops as the LDPE substrates rotate. It is clear that, for the 4 μL and 10 μL volumes, the drops do not roll off even if the surface is tilted at 90° and it is only the drops of 20 μL and 30 μL volume that roll off at 41° and 26°, respectively. At an angle just one degree before rolling, the difference between the advancing and the receding angles defines the contact angle hysteresis for the specific substrate and in this case is calculated to be ~19°. Therefore, neat LDPE is a slightly hydrophobic surface with significant water adhesion. This is illustrated in the Video S1 of the ESI‡ as well.

The thermal properties of the LDPE film were measured using DSC and its melting and crystallization temperatures were determined as T_m = 111 ± 1 °C and T_c = 101 ± 1 °C in good agreement with the literature values;[87] the respective measurement is shown as Fig. S1a in the ESI.‡ The optical properties of the film were measured by UV-vis spectroscopy

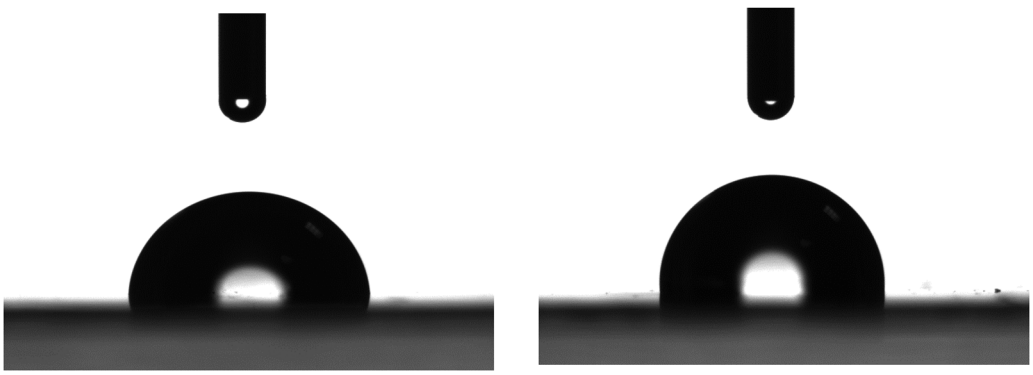

Fig. 1 Photographs of representative water drops of 4 μL deposited on different positions of a flat LDPE film.

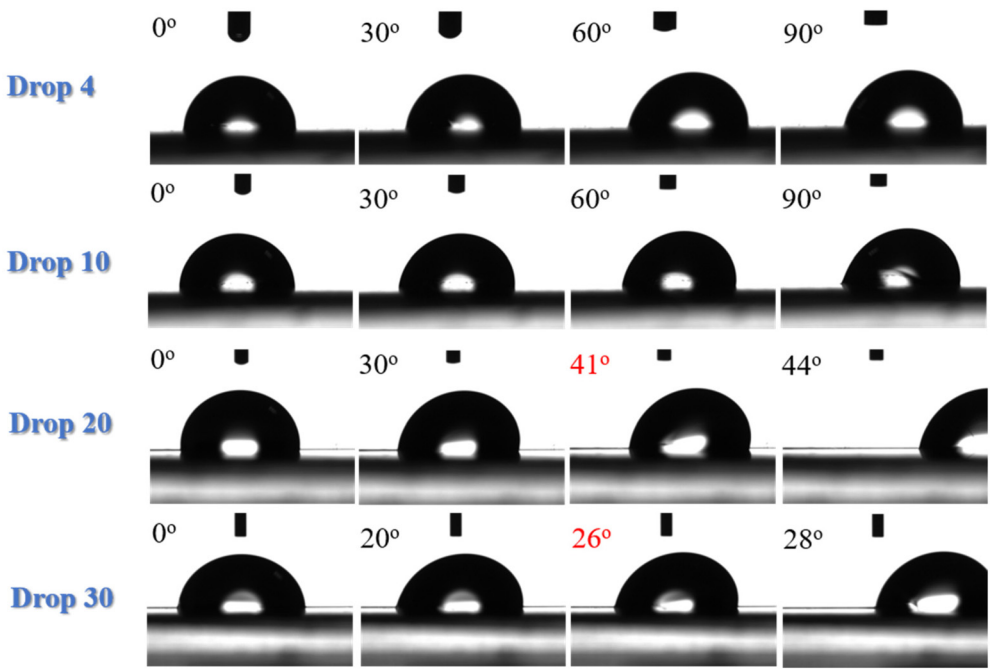

Fig. 2 Measurements of the roll off angles for water drops of 4, 10, 20 and 30 μL (from top row to bottom) on a neat LDPE film. The red numbers on the up left corner shows the roll off angle for the 20 μL and 30 μL droplets, which are 41° and 26°, respectively.

(Fig. S2 in the ESI‡) and showed 90% transmittance over the whole wavelength regime investigated.

LDPE is a non-polar polymer with no functional groups that could interact favourably with other (macro)molecules. In order to be able to prepare a stable coating on an LDPE film, its surface should be modified to increase its surface energy. To achieve this, the LDPE films underwent a corona treatment, which is a surface modification technique frequently used to facilitate the deposition of waterborne solutions on hydrophobic films. It uses a low temperature corona discharge plasma to impart changes in the properties of a surface. The plasma is generated by the application of high voltage to a linear array of sharp tip electrodes. During the corona treatment, polar hydroxyl, carbonyl and carboxyl groups are formed on the LDPE surface, thus, increasing its surface energy. Fig. 3 shows representative photographs of water drops deposited on the corona treated LDPE film. It is obvious that, following the corona treatment, the LDPE film becomes more hydrophilic since the water drops now wet the surface with contact angles of 55 ± 3° measured ~40 min after the corona treatment; this value increases with time when the surface remains at ambient conditions and stabilizes at a value of ~70 ± 3° after 26 h due to the attachment of hydrophobic impurities from the environment. The contact angle remains constant at this value even 20 days later.

The hydrophilic character of the LDPE corona is confirmed by the measurement of the water roll off angles as well. Fig. 4 shows water drops of different volumes (4, 10, 20, 30 and 35 μL) deposited on LDPE corona treated surfaces that are tilted up to 90°. No movement of the drop can be observed even when the surface is in the vertical direction not only for the smaller drops (as in the untreated LDPE) but for the 20 μL drop as well. It is only for the larger (30 μL) drops that rolling is observed at an angle of 53°, which is much higher than the respective angle of 26° measured for neat LDPE. A high roll off angle of 36° is observed even for the water drop of 35 μL, which was the largest drop volume used. This behaviour is attributed to the hydrophilic character of the corona treated LDPE surface that demonstrates strong adhesion with water preventing the rolling of the drops and the increase of the contact angle hysteresis, which has reached values of ~30°.

The morphology of the LDPE surface prior and after the corona treatment was examined using SEM and representative images are shown in Fig. 5.

A uniform surface was observed in both cases with no important heterogeneities; its roughness was estimated, using surface profilometry, at ~0.3 μm and ~0.4 μm before and after the corona treatment, respectively, indicating that the procedure for the surface modification influences only its composition and not its topology.

3.2. Nanohybrid coatings with silanes/siloxanes and silica nanoparticles

Waterborne nanohybrid coatings were developed to be deposited onto the flexible polymer films; the coatings should contain proper film-forming organic agents that would provide the appropriate hydrophobicity as well as nanoparticulate additives that would provide the appropriate multiscale roughness. The first system investigated is a commercial one, Silres BS 4004, which is an emulsion containing mixture of silanes and siloxanes, *i.e.*, molecules of low surface energy. These molecules have the ability to form a hydrophobic silicone film when deposited on a surface containing hydroxyl groups. Dynamic Light Scattering measurements showed that the emulsion contains scattering moieties ("particles") with a hydrodynamic radius of R_h = 85 nm, whereas DSC measurements (shown in Fig. S3 in ESI‡) did not reveal any thermal transition in the temperature range 0–200 °C.

FTIR-ATR measurements were performed to verify the formation of the Silres BS 4004 coating onto the film surface and its possible interaction with the LDPE substrate. Fig. 6 shows the spectra for the uncoated corona treated LDPE films and for the substrate following the dipping in the Silres dispersion.

As can be seen in the ATR-FTIR spectra of Fig. 6, LDPE exhibits four characteristic peaks attributed to the $-CH_2$ rocking at 719 cm^{-1}, the $-CH_2$ symmetric wagging at 1360 cm^{-1} or the –CC stretching at 1360 cm^{-1}, and the CH_2 antisymmetric bending, and symmetric/antisymmetric stretching at 2850/2910 cm^{-1}. In the spectrum of the sample coated with 2 wt% Silres BS 4004, characteristic bands that correspond to Si–O or Si–C vibrations can be identified in the range between 800–1250 cm^{-1}, due to the presence of the Silres on the

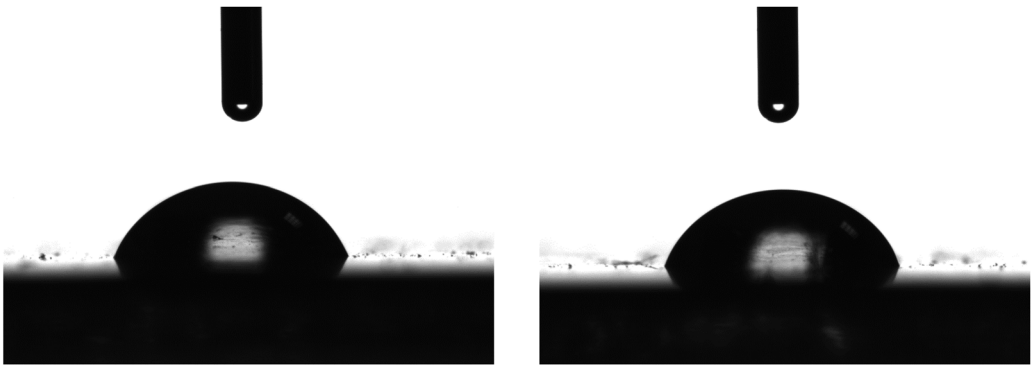

Fig. 3 Representative photographs of 4 μL water drops on different positions of a corona treated LDPE films.

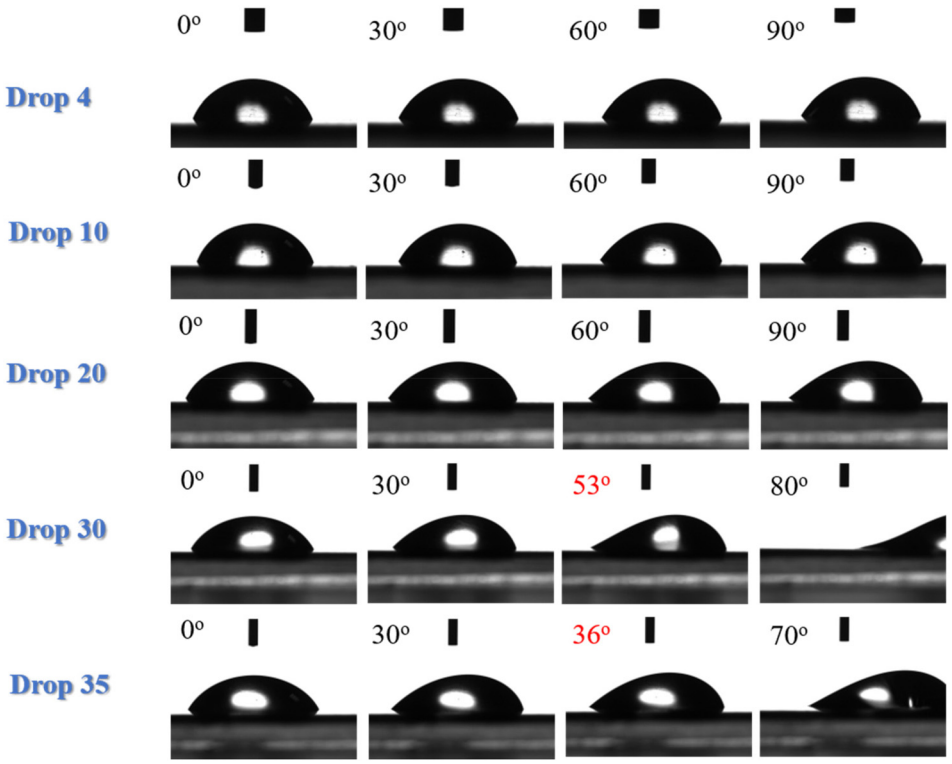

Fig. 4 Measurements of the roll off angles for water drops of 4, 10, 20, 30 and 35 μL (from top row to bottom) on a corona treated LDPE film. The red numbers on the up left corner shows the roll off angle for the 30 μL and 35 μL droplets, which are 53° and 36°, respectively.

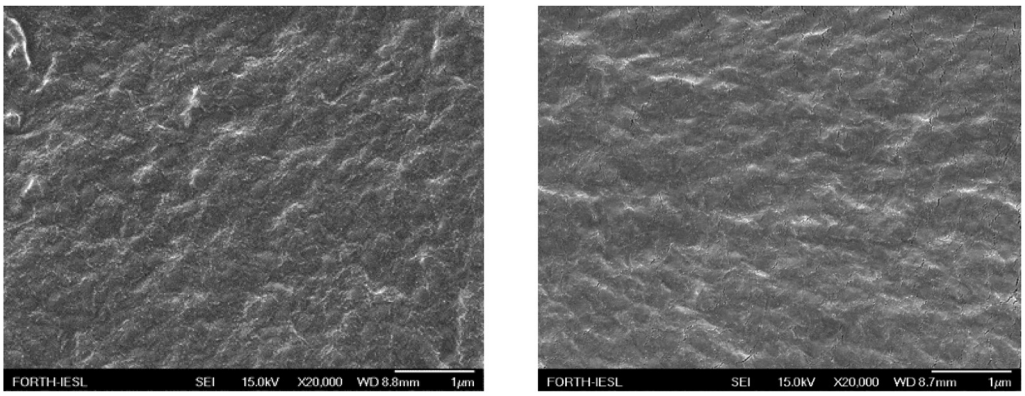

Fig. 5 SEM images of a neat LDPE film surface (left) and a LDPE film after corona treatment (right).

polymer substrate. Moreover, the Si–O stretching vibration observed at 1105 cm^{-1} and 1025 cm^{-1} is attributed to Silres molecules that are chemically bonded to each other and/or to the corona treated substrate. Despite the low intensity of the bands, probably because of the small thickness of the coating, their presence proves that the coating is present onto the polymer surface.

Additionally, X-ray Photoelectron Spectroscopy, XPS, measurements were performed on the bare and the Silres coated LDPE substrate and the measurements are shown in Fig. S4 of the ESI.‡ In the spectrum of the corona treated LDPE, two peaks can be observed at binding energies 284.5 and 530.8 eV corresponding to the C1s and O1s with relative percentages 82.2 : 17.8. In the case of the corona treated LDPE that was coated with a Silres BS 4004 dispersion of 2 wt% in water, extra peaks at binding energies 99.9 eV and 150.9 eV are observed, which correspond to Si 2s and Si 2p photoelectron peaks. The surface atomic composition of the coated surface is calculated as C : O : Si = 58.7 : 22.7 : 18.6. All compositions are reported in Table S1 of the ESI.‡

Emulsions of different concentrations of Silres BS 4004 were utilized to deposit coatings of different thicknesses onto

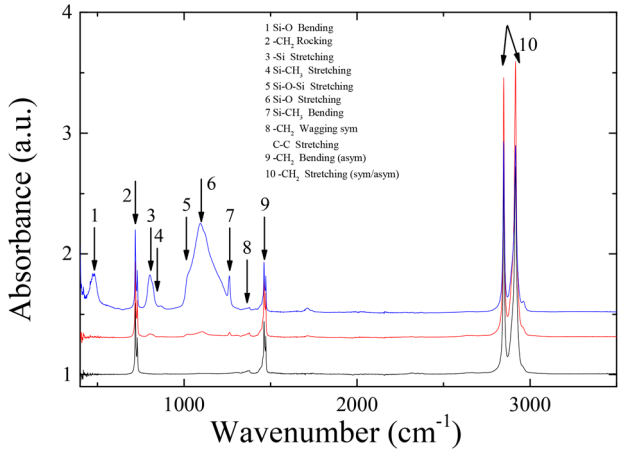

Fig. 6 ATR-FTIR spectra of corona treated LDPE film (black), corona treated LDPE coated with Silres of 2 wt% concentration in water (red) and corona treated LDPE coated with the nanocomposite Silres/ZL 77%/23% (blue).

the LDPE substrates, which had undergone corona treatment. Fig. 7 shows the dependence of the water contact angle onto these coatings measured as a function of Silres BS 4004 concentration.

A non-monotonic dependence of the contact angle on the Silres BS 4004 content is observed. For low Silres BS 4004 concentrations, the presence of the coating causes an increase of the contact angle values by approximately 30° in comparison to the corona treated LDPE film, thus converting the surface to a hydrophobic one. However, further increase of the concentration results in a significant decrease of the contact angles probably because of the large number of Si–OH groups of the Silres BS 4004, which remain in excess on the surface and, therefore, decrease its hydrophobicity. The Silres concentration that resulted in the most hydrophobic surface with a maximum contact angle of 103 ± 2° was that of 2 wt% Silres BS 4004 in water. Hysteresis measurements for the specific substrate showed that a water drop of 20 μL rolls off at a tilting angle of 51°. It is, thus, concluded that coating the LDPE film with Silres enhances its hydrophobicity resulting in a contact angle higher than 100° and a hysteresis lower than that of the LDPE film after the corona treatment. Fig. 8 shows SEM images of the LDPE film coated with 2 wt% Silres BS 4004, which reveals the presence of a uniform coating; its roughness is estimated ~0.9 μm based on profilometry measurements.

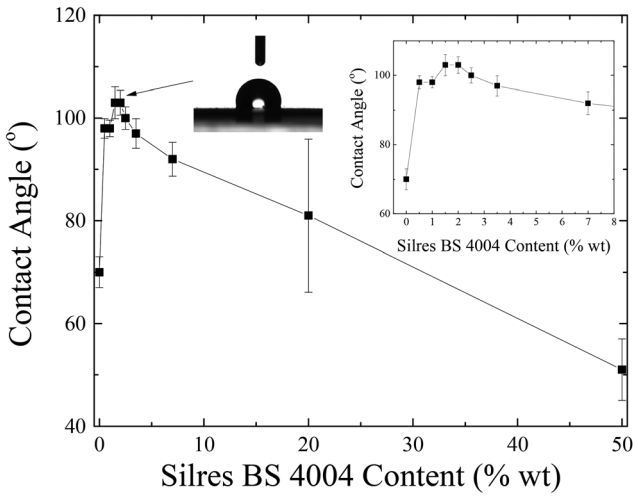

Fig. 7 Equilibrium contact angles of water drops measured onto corona treated LDPE substrates coated with Silres BS 4004 as a function of Silres BS 4004 concentration in water. The insets show enlarged the low concentration regime as well as a representative photograph of a water drop on the surface coated with Silres BS 4004 at 2 wt% concentration, *i.e.*, for the surface that exhibits the maximum contact angle.

In order to enhance further the hydrophobicity of the coated LDPE films, nanoparticles were introduced in the coating formulations in order to modify the roughness of the surface in the nanoscale, in excess of the inherent roughness of the polymer film, which was in the μm scale. Thus, the coating would now exhibit multiscale roughness in the micro- and in the nano-scale. To achieve this, a nanocomposite coating was prepared based on the Silres BS 4004 emulsion with 2 wt% concentration in water, which was the one that exhibited the most hydrophobic behaviour upon coating the LDPE surface, and silica nanoparticles. The SiO_2 nanoparticles selected were the Snowtex ZL having a radius of R = 67 nm (as measured by DLS and TEM) and dispersions with different Silres/SiO_2 compositions were prepared and deposited onto the corona treated LDPE surfaces. ATR-FTIR measurements were performed in this case as well and they are also shown in Fig. 6. The characteristic bands discussed above for the Silres coated surface can be observed in this case as well; however, the –Si related bands (Si–O, Si–Si) can be observed more pronounced, due to the presence of the silica nanoparticles in the coating.

Fig. 9 shows the dependence of the contact angle of the LDPE surfaces coated with the nanohybrids, as a function of the composition of the coating. For low concentration of nanoparticles, their presence does not really influence the values of the contact angles, which remain similar with the ones of the neat Silres coated film. However, for a nanohybrid coating with more than 50 wt% of nanoparticles, a significant increase of the contact angles is observed that reach values of 135 ± 1°. Moreover, hysteresis measurements showed that water droplets can roll off the surface even for moderate hydrophobicity, *i.e.*, below 50 wt% nanoparticles. For example, for 23 wt% ZL, rolling angles of 30° and 21° are observed for water drops of 20 μL and 30 μL, respectively. Rolling is observed even for the smaller water drops (10 μL) at 44°. Similar results are obtained for a hybrid coating with 33 wt% of nanoparticles; in both cases, the average hysteresis is calculated to be lower than 17°. However, for compositions higher in nanoparticles, despite the significant increase of hydrophobicity, even a large water drop cannot roll off the surface as shown in the Video S2 of the ESI,‡ *i.e.*, the surface shows a larger hysteresis even compared to the neat LDPE, which corresponds to a surface with significant water adhesion. Therefore, coating composition

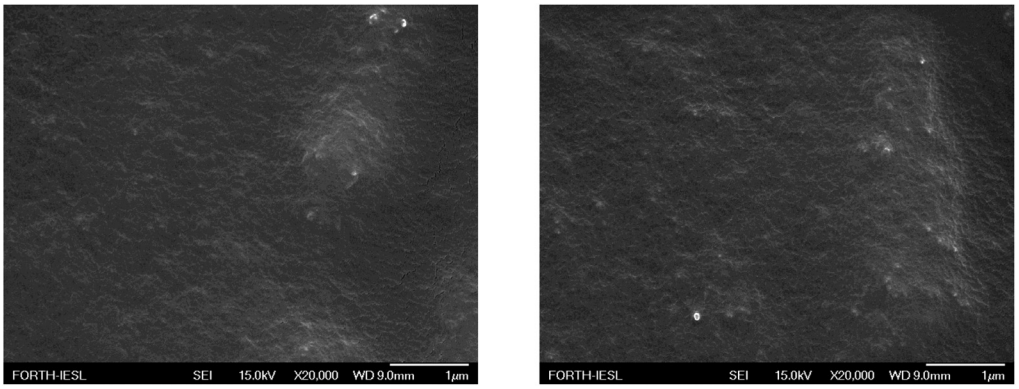

Fig. 8 SEM images of the LDPE films, coated with Silres BS 4004 with concentration 2 wt% in water, at different positions.

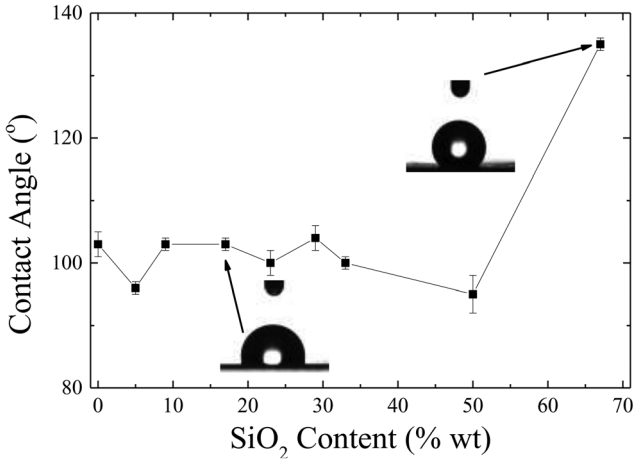

Fig. 9 Equilibrium water contact angles measured for coated LDPE film surfaces utilizing aqueous dispersions, which contain Silres BS 4004 (2 wt% in water) and Snowtex ZL silica nanoparticles as a function of the concentration of the nanoparticles in the coating. Photographs of water droplets are shown for two different concentrations to demonstrate the different surface properties of the coated LDPE films.

affects both the hydrophobicity and the water adhesion of the surface in a non-monotonous way and one should carefully choose the correct system depending on the desired application.

Fig. 10 shows the surface morphology of LDPE surfaces after the deposition of nanocomposite coatings with 33 wt% (Fig. 10, left) and 67 wt% (Fig. 10, right) nanoparticles. The surfaces appear very rough; however, they exhibit uniform characteristics, which are responsible for the manifestation of the observed surface properties.

It is noted that the surface properties of the coated LDPE remain unchanged even after thermal annealing at 90 °C overnight. Moreover, the presence of the nanocomposite coating does not affect the thermal and optical properties of LDPE as shown in Fig. S1b and S2, respectively, of the ESI.‡

A similar study, like the one discussed above, was carried out utilizing Silres BS 4004 and SiO_2 nanoparticles of smaller size (particle radii R = 7 nm and 14.5 nm, respectively). In those cases, the film surfaces coated with the nanohybrid coatings containing ~30 wt% nanoparticles were found almost superhydrophobic, since they showed contact angles even up to 140°, however, with relatively high hysteresis of ~50°. Nevertheless, following thermal annealing of the surfaces at 90 °C, the contact angles decrease to ~100°, similar to neat Silres BS 4004 and, thus, these surfaces were not studied further.

3.3. Nanohybrid coatings with a fluoroalkyl silanol and alumina nanoparticles

The second system investigated is also based on a commercial one that utilizes a fluoroalkyl silanol as the low surface energy material. The material used is Dynasylan SIVO 121, which contains three silanol groups and a fluoroalkyl chain with 4 to 6 fluorine atoms; it is stabilized in an aqueous solution at low pH. Investigation of its thermal properties reveals no thermal transitions in the temperature range between 0–200 °C (Fig. S5 of the ESI‡). It is noted that Dynasylan SIVO 121 is commercially available as a ready to use aqueous solution with 2 wt% concentration; however, it was diluted in various concentrations to fabricate polymer coatings of different thicknesses on the LDPE substrates. The coatings were deposited *via* the dipping method. ATR-FTIR measurements (Fig. 11) were performed in this case as well, to verify the presence of the coating onto the substrate. For the substrate coated with Dynasylan SIVO 121, the characteristic bands of LDPE as well as the Si–O and Si–C vibrations at 800–1250 cm^{-1}, which were already discussed in relation to Fig. 6, can be also observed, while the appearance of additional bands at 1100–1400 cm^{-1} is associated with $-CF_2$ and CF vibrations. The bands of the Si–O or Si–C vibrations are attributed to the silanol groups of Dynasylan and those of the $-CF_2$ and CF vibrations to its fluoroalkyl chain.

Additionally, XPS measurements were performed on a film coated with the Dynasylan SIVO 121 of 1 wt% concentration in water and the results are shown in Fig. S6 and Table S1 of the ESI‡ together with the respective ones for the neat corona treated LDPE for comparison. Photoelectron peaks at binding energies 99.9 eV and 150.9 eV are observed and identified as

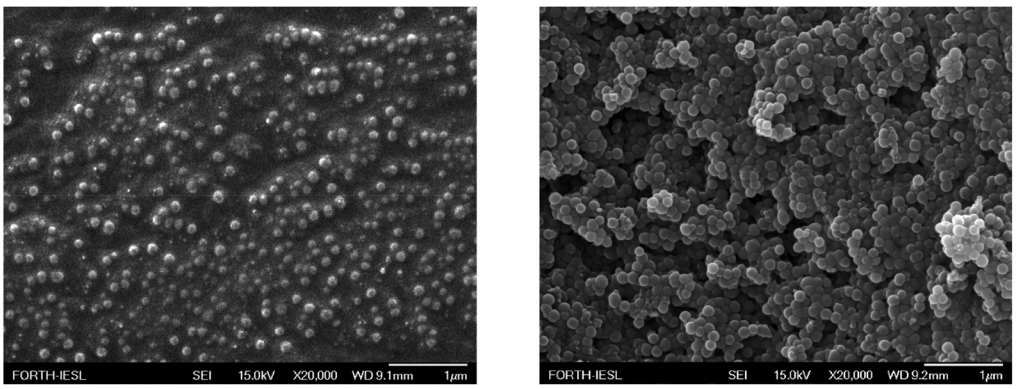

Fig. 10 SEM images of LDPE films, after the deposition of a nanocomposite coating consisting of (left) 67 wt% Silres BS 4004 and 33 wt% ZL nanoparticles and (right) 33 wt% Silres BS 4004 and 67 wt% ZL nanoparticles.

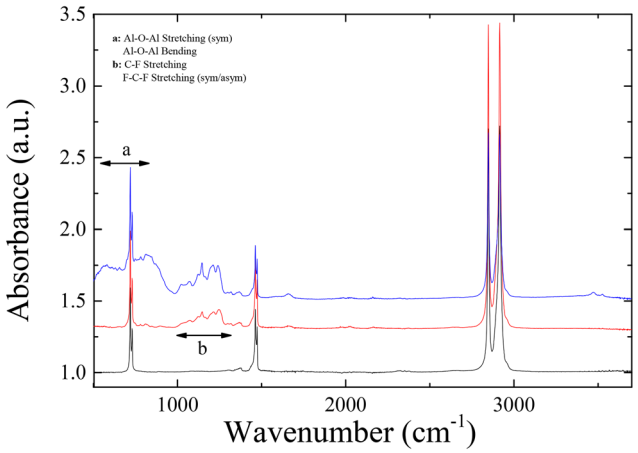

Fig. 11 ATR-FTIR spectra of corona treated LDPE (black), corona treated LDPE coated with Dynasylan SIVO 121 of 1 wt% concentration in water (red) and corona treated LDPE coated with the nanocomposite Dynasylan SIVO 121/PG003 66%/34% (blue).

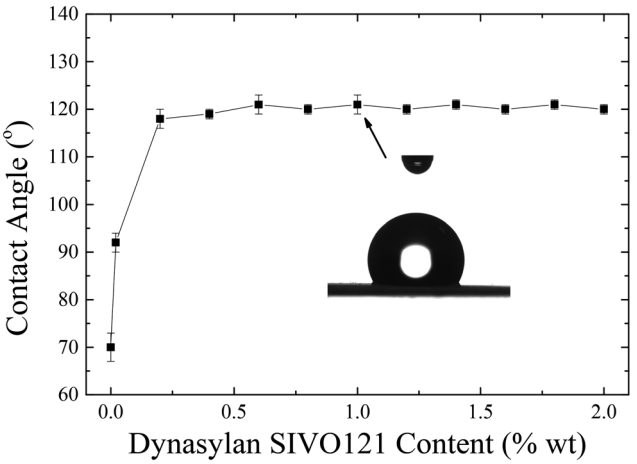

Fig. 12 Equilibrium contact angles of water drops measured onto corona treated LDPE substrates coated with Dynasylan SIVO 121 films as a function of the Dynasylan concentration in water. The inset shows a photograph of a water drop on the surface coated with Dynasylan at 1 wt% concentration.

the Si 2s and Si 2p peaks and at binding energy 684.9 eV attributed to F 1s. The atomic chemical composition of the coated surface is calculated as C : O : Si : F = 27.9 : 7.2 : 3.9 : 61.0.

Fig. 12 shows the values of the contact angles of water drops on the corona treated LPDE film surfaces coated with Dynasylan SIVO 121 from solutions of different concentrations.

An increase in the water contact angles is observed with the coating, which reaches values above 90° even when the LDPE film is dipped in a very dilute solution (0.02 wt%). Further increase of the concentration above 0.2 wt% results in even larger increase of the contact angles, which reach and remain constant at values ~120°; it is noted that this value is much higher than the respective one obtained utilizing Silres BS 4004 which was ~103°. As mentioned above, Dynasylan is an fluoroalkyl silanol and, when deposited on a corona treated LDPE film, condensation reactions take place between the hydroxyl groups of Dynasylan and the functional groups of the corona treated LDPE. Through these reactions, the fluoroalkylsilanol binds onto the polymer substrate and its fluorine atoms, being very hydrophobic, remain on the surface, thus, resulting on the significantly high values of the water contact angles.

To further increase the water contact angles on the LDPE substrates, an increase of its hierarchical roughness was attempted *via* the addition of nanoparticles in the Dynasylan solution; the solution of Dynasylan 1 wt% was chosen for the preparation of the nanocomposite coatings. Because of the low pH of the polymer solution, the nanoparticles used were alumina nanoparticles of radius R = 75 nm with the commercial name PG003. These nanoparticles are provided in the form of a dispersion at a pH of ~4.2 in water and, thus, they can form a stable dispersion in the aqueous solution of Dynasylan SIVO 121. The presence of the alumina nanoparticles in the nanocomposite coating was confirmed *via* ATR-FTIR by the appearance of broad bands in the lower wave-

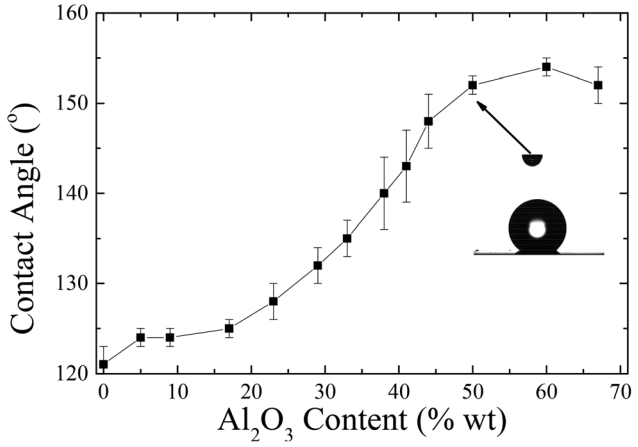

Fig. 13 Equilibrium water contact angles measured for corona treated LDPE film surfaces coated utilizing aqueous dispersions containing Dynasylan SIVO (at 1 wt%) and PG003 alumina nanoparticles as a function of the concentration of the nanoparticles in the coating. A photograph of a water droplet is shown for a 50 wt% concentration of the nanoparticles.

number range (550–800 cm^{-1}), as well as by the characteristic peak at 3400 cm^{-1}, as shown in Fig. 11.

Fig. 13 shows the water contact angle of corona treated LDPE substrates coated with the nanocomposites containing 1 wt% Dynasylan and PG003 at different nanoparticle concentrations.

Increasing the alumina content (up to 20 wt%) results in a weak increase of the contact angles by ~5°; further increase of the concentration of nanoparticles leads to a more abrupt increase with water contact angles reaching a maximum of 154 ± 1° at 60 wt% PG003.

For nanohybrid coatings with nanoparticle concentrations higher than 44 wt% in nanoparticles, a superhydrophobic behaviour is observed. For these surfaces, a contact angle hysteresis of less than 5° is measured; thus, these surfaces can be classified as both superhydrophobic and water-repellent. Fig. 14 shows snapshots that demonstrate the bouncing and rolling off of a water droplet of 10 μL from a corona treated LDPE surface subsequently coated with a 56 wt% Dynasylan and 44 wt% PG003 nanohybrid film at a tilting angle of 5°. Video S3a of the ESI‡ shows the respective video whereas Video S3b‡ demonstrates how a water drop is completely repelled and is not able to even sit on a horizontal surface.

It is noted that thermal annealing of the coated surfaces at 90 °C do not alter the behaviour, which remains superhydrophobic and water-repellent. For example, for the surface that is coated with 56 wt% Dynasylan and 44 wt% PG003, the water contact angle becomes 149 ± 3° after annealing (it was 148° before) and the contact angle hysteresis remains less than 5°.

Fig. 15 shows a SEM image of the surface morphology of a LDPE substrate coated with 56 wt% Dynasylan SIVO 121 and 44 wt% PG003. It is clear that the surface topology, although rough, is very uniform, which justifies the manifestation of the observed surface behaviour. Further than the average roughness in the scale of μm of the coated LDPE, measured by profilometry to be ~2 μm, the presence of the alumina nanoparticles covering the entire surface and providing the extra roughness in the range of a hundred nanometers is obvious.

The oleophobicity of the coated LDPE surfaces was examined as well. Fig. 16 shows photographs of drops of three different organic solvents, glycerol, 1,2-ethylene glycol and dimethylsulfoxide (DMSO), on a LDPE substrate coated with the nanocomposite containing 56 wt% Dynasylan and 44 wt% PG003 film. For all three solvents, the contact angles have increased significantly after the deposition of the coating when compared with the neat LDPE film, similarly to the case of water.

Table 1, summarizes the results concerning the contact angles for the three organic solvents together with the respective ones for water on the neat LDPE film surfaces and on surfaces coated with 56 wt% Dynasylan and 44 wt% PG003. It is obvious that the coated LDPE surface is superhydrophobic and, at the same time, superoleophobic for glycerol and strongly oleophobic for 1,2-ethylene glycol. Even in the case of DMSO the surface is slightly oleophobic.

Finally, the UV-vis and DSC measurements confirmed that the optical and thermal properties of the coated polymer films were not influenced by the presence of the coating. UV-vis

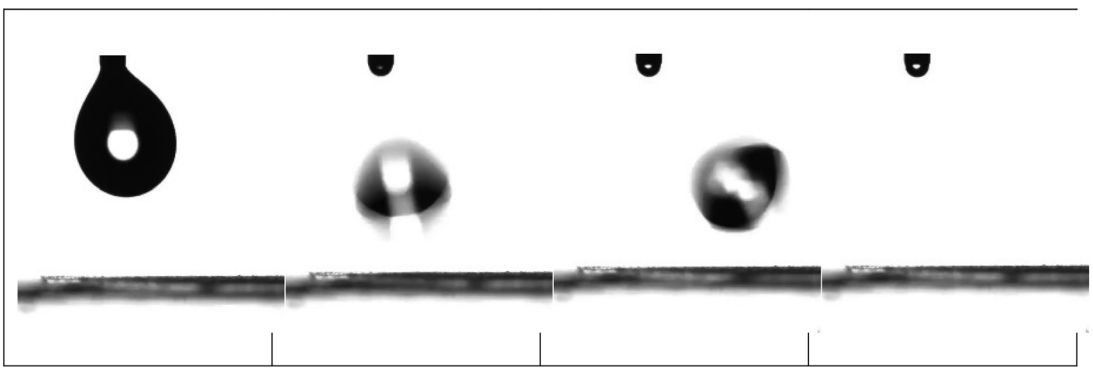

Fig. 14 Water repellence of a LDPE substrate coated with a nanohybrid film of 56 wt% Dynasylan SIVO 121 and 44 wt% PG003.

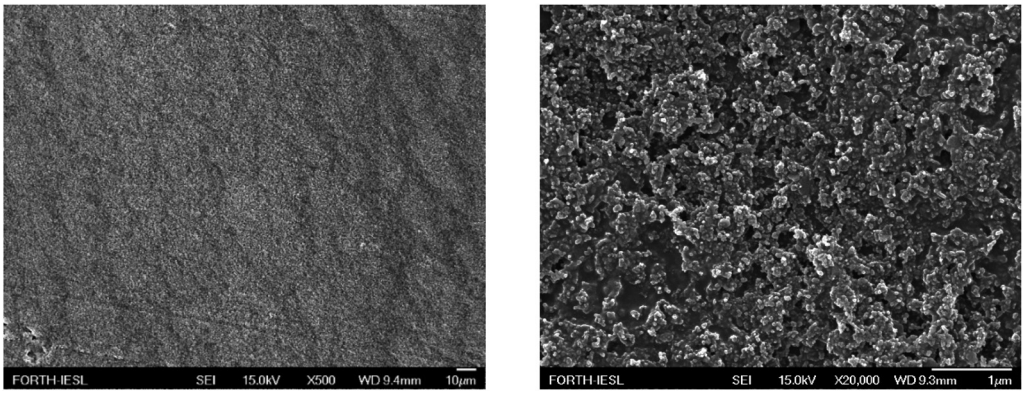

Fig. 15 SEM images of a LDPE substrate following the coating with a 56 wt% Dynasylan Sivo 121 and 44 wt% PG003 nanohybrid film in (left) low and (right) high magnification.

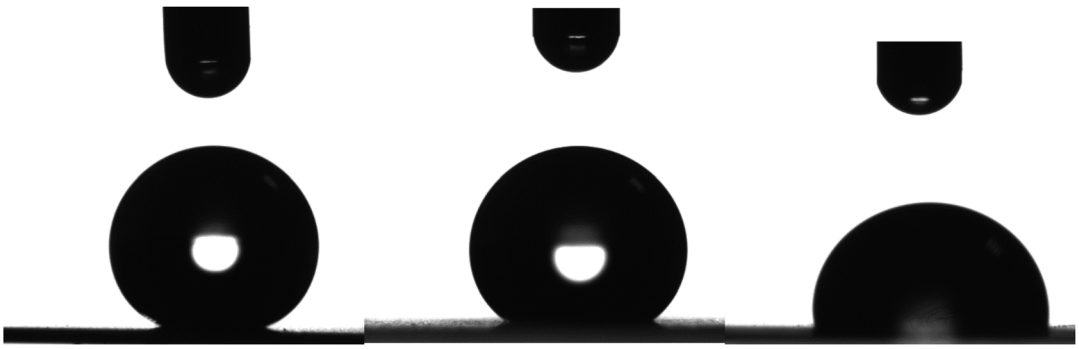

Fig. 16 Photographs of 4 μL droplets of (left) glycerol, (center) 1,2-ethylene glycol and (right) DMSO on a LDPE substrate coated with a nanocomposite coating containing 56 wt% Dynasylan SIVO 121 and 44 wt% PG003.

Table 1 Contact angles of drops of water and three organic solvents (glycerol, 1,2-ethylene glycol and dimethylsulfoxide) on the neat LDPE film surface and on surfaces coated with a nanocomposite coating containing 56 wt% Dynasylan and 44 wt% PG003

	Water contact angle	Glycerol contact angle	1,2-Ethylene glycol contact angle	Dimethylsulfoxide contact angle
Neat LDPE	97 ± 3°	82 ± 1°	74 ± 2°	57 ± 3°
Coated LDPE	148 ± 3°	150 ± 1°	138 ± 2°	96 ± 3°

showed a transparency of about 90% over the optical spectrum (Fig. S2 in the ESI‡), whereas the DSC thermograph revealed a crystallization temperature of the coated LDPE of 98 °C and a melting temperature of 108 °C.

3.4. Mechanical and chemical durability of the coated films

The mechanical and chemical durability of the coated LDPE surfaces was investigated in comparison to the uncoated LDPE substrates. Fig. 17 shows stress-strain curves of the corona treated LDPE together with the films that were coated with the Silres BS 4004 and Dynasylan SIVO 121 and their nanocomposites.

In all cases, it is clear that the elastic regime is very similar between the neat and the coated LDPE films. A notable increase of both the stress and the strain at break is observed (Fig. 17a) for the film coated with Silres when compared to neat LDPE (from 575% to 780% for the strain). The increase is even higher for the film with the nanocomposite coating (a slight decrease in the stress at break is observed in this case), which reveals an elongation before break of about 880%. Such results indicate that the presence of Silres and the silica nanoparticles enhance the mechanical properties of the polymer. This is most probably due to the formation of a crosslinked network of a silicone film onto the LDPE surface, as anticipated.

For the Dynasylan SIVO 121 coated films (Fig. 17b), the stress–strain curves show a behavior similar to the neat LDPE, indicating that the deposition of the Dynasylan and its nanocomposite with alumina nanoparticles have no significant effect on the mechanical behavior of LDPE.

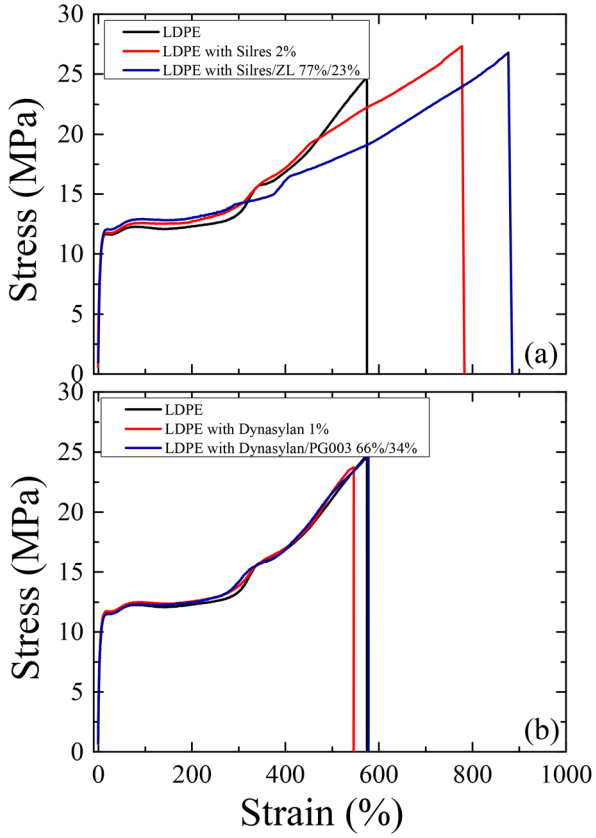

Fig. 17 Stress – Strain curves of (a) corona treated LDPE coated with Silres of 2 wt% concentration in water (red) and corona treated LDPE coated with the nanocomposite Silres/ZL 77%/23% (blue) and (b) corona treated LDPE coated with Dynasylan SIVO 121 of 1 wt% concentration in water (red) and corona treated LDPE coated with the nanocomposite Dynasylan SIVO 121/PG003 66%/34% (blue). In both (a) and (b) the respective stress – strain curve of uncoated corona treated LDPE is shown as black line.

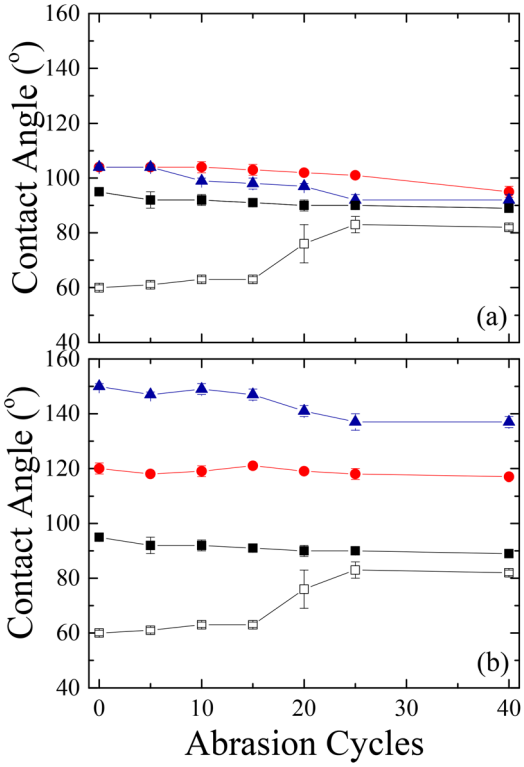

Fig. 18 Water contact angle measurements following sandpaper abrasion tests for (a) corona treated LDPE coated with Silres BS 4004 2 wt% concentration in water (red circles) and with the nanocomposite Silres/ZL 77%/23% (blue triangles) and (b) corona treated LDPE coated with Dynasylan SIVO 121 1 wt% concentration in water (red circles) and with the nanocomposite Dynasylan/PG003 66%/34% (blue triangles). The corresponding measurements for the neat untreated and the corona treated LDPE are shown in both (a) and (b) for comparison as filled and empty black squares, respectively.

The scratch resistance of the films was evaluated as well *via* a sand paper abrasion test. Fig. 18 shows the results of the abrasion tests on surfaces coated with Silres BS 4004 and Dynasylan SIVO 121 and their nanocomposites in comparison with the neat LDPE and the corona treated one.

The abrasion durability tests of the neat LDPE (Fig. 18a) revealed that the untreated film is insensitive to the abrasion since the values of the water contact angles remain almost constant at ~90° even after 40 cycles; however, the data for the corona treated film show that the functionalization of the surface is destroyed after 15 cycles, as the contact angles increase by ~20° and reach almost the values measured for neat LDPE. Moreover, in the latter case, the optical properties of the substrate degrade after 5 cycles and the film becomes hazy. On the other hand, the water contact angles for the sample coated with Silres BS 4004 remain constant for up to ~25 abrasion cycles; at that point, a small decrease of the contact angle by ~6° was observed. As far as the transparency of the coated film is concerned, no blurring was noticed up to ~15 cycles. For the substrate coated with the nanocomposite Silres/ZL 77%/23%, a systematic decrease of the contact angle by ~10° was observed between cycles 5–25; at the end, the contact angle value remained constant at ~92°, close to the values for the untreated LDPE.

For the films coated with either Dynasylan SIVO 121 or its nanocomposites, the results revealed a significant difference from the situation described above (Fig. 18b). More specifically, the surface coated with the Dynasylan SIVO 121 showed no change to the measured water contact angle even after 40 cycles. Moreover, the surface coated with the Dynasylan/PG003 nanocomposite remained superhydrophobic and water repellent for up to 15 abrasion cycles (~147°). Even after 40 cycles the coating remained strongly hydrophobic with a contact angle of 137°. This means that the interactions between the alumina nanoparticles, the fluoropolymer and the substrate are stronger and that the specific coating is more strongly bonded to the surface than the respective ones with Silres. Additionally, the optical properties do not seem to be affected by the abrasion in this case since no increase in the hazeness was observed after 40 cycles. These properties make this coated film a good candidate for many applications.

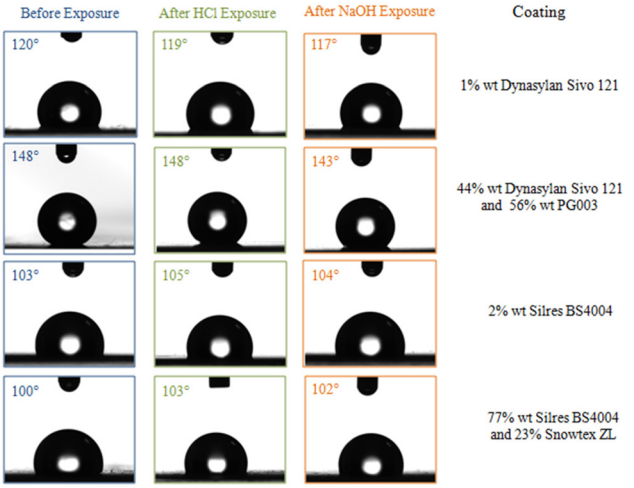

Fig. 19 Water contact angles of the coated LDPE films before and after exposure at acidic and basic environment.

Finally, the chemical durability of the investigated coatings was investigated as well. It is noted that the dispersions of the nanocomposite coatings are at pH = 5 and pH = 8 for Dynasylan SIVO 121/PG003 and Silres BS 4004/ZL, respectively. The durability of the coated films that showed the optimum surface properties in both cases was tested in highly acidic and highly basic pH using HCl 0.1 M to reach pH = 1.5 and NaOH 0.1 M to reach pH = 13. The contact angles were measured for each film (for water drops of 4 μL in volume) before and after being submerged in the acidic or basic solution. Representative contact angle measurements before and after being exposed to the acidic and basic conditions are shown in Fig. 19. It is clear that the wetting properties were not especially affected in none of the cases.

4. Conclusions

The present work demonstrates the development of polymer films with superhydrophobic characteristics, utilizing nanocomposite coatings. The first system investigated was an emulsion of silanes and siloxanes, identified by the commercial name Silres BS 4004, mixed with silica nanoparticles, that was deposited on corona-treated LDPE substrates by dipping. It was found that, although the contact angle showed only a small increase, the substrates revealed a tendency of water droplets to roll off the surface with rather low roll off angles.

The second nanocomposite system used was an aqueous solution of a fluoroalkyl silanol, identified as Dynasylan SIVO 121, mixed with alumina nanoparticles. In this case, depending on the nanoparticle content, the coated substrates became superhydrophobic and water repellent with roll off angles lower than 5°. Moreover, these coatings enhanced the oleophobicity of the LDPE, showing superoleophobicity for glycerol and an increase of the contact angle by 40°–70° for other organic solvents. Furthermore, it was found that the polymer films have a significant robustness to temperature and their surface properties are not affected by annealing procedures. Moreover, the coated surfaces show similar or even better mechanical properties, scratch resistance and chemical durability in comparison to the neat LDPE film. Finally, the optical and thermal properties of LDPE are not affected by the presence of the nanocomposite coatings and remain similar to neat polymer.

These coatings can be ideal candidates for applications on polymer films used in greenhouses. The treatment with the nanocomposite coatings can transform their surfaces to self–cleaning ones with antidust properties, without affecting the optical and thermal properties of the original polymer film. Moreover, their thermal robustness to temperature makes them suitable for application to even extreme external conditions.

Author Contributions

Conceptualization, K. C. and S. H. A.; methodology, F. K. and K. C.; measurements and analysis, F. K. and M.-Th. Ch.; measurement supervision, F. K. and K. C.; writing – original draft preparation, F. K. and M.-Th. Ch.; writing – review and editing, K. C. and S. H. A.; project administration, K. C. and S. H. A.; funding acquisition, S. H. A. All authors have read and agree to the published version of the manuscript.

Conflicts of interest

The authors declare no conflicts of interest.

Acknowledgements

This research has been co-financed by the European Union and Greek national funds through the Operational Program Competitiveness, Entrepreneurship and Innovation, under the call RESEARCH–CREATE–INNOVATE administered by the General Secretariat of Research and Innovation (project INGRECO, project code: T1EDK-01499, MIS: 5030174). The authors acknowledge our collaborators at Plastika Kritis S. A., Dr Michalis Kapnistos and Mr Pithagoras Fragiadakis, for providing the neat LDPE films as well as for performing the corona treatment. The authors acknowledge the help of Ms Alexandra Manousaki with the SEM measurements, Ms Katerina Stamataki with the ATR-FTIR measurements, Ms Manolis Stratakis and Mr Ioannis Karnis with the XPS measurements and analysis. Elton Group and Safic Alcan Hellas are highly acknowledged for providing Silres BS 4004 and Dynasylan SIVO 121, respectively.

References

1 S. H. Anastasiadis, *Langmuir*, 2013, **29**, 9277–9290.
2 S. G. Moghadam, H. Parsimehr and A. Ehsani, *Adv. Colloid Interface Sci.*, 2021, **290**, 102397.

3 J. Peng, X. Zhao, W. Wang and X. Gong, *Langmuir*, 2019, **35**, 8404–8412.
4 I. P. Parkin and R. G. Palgrave, *J. Mater. Chem.*, 2005, **15**, 1689–1695.
5 K. Liu and L. Jiang, *Annu. Rev. Mater. Res.*, 2012, **42**, 231–263.
6 A. G. Nurioglu, A. C. C. Esteves and G. de With, *J. Mater. Chem. B*, 2015, **3**, 6547–6570.
7 Z. He, X. Lan, Q. Hu, H. Li, L. Li and J. Mao, *Prog. Org. Coat.*, 2021, **157**, 106285.
8 M. Ferrari and A. Benedetti, *Adv. Colloid Interface Sci.*, 2015, **222**, 291–304.
9 L. Ionov and A. Synytska, *Phys. Chem. Chem. Phys.*, 2012, **14**, 10497–10502.
10 C. Zhang, F. Liang, W. Zhang, H. Liu, M. Ge, Y. Zhang, J. Dai, H. Wang, G. Xing, Y. Lai and Y. Tang, *ACS Omega*, 2020, **5**, 986–994.
11 X. Han and X. Gong, *ACS Appl. Mater. Interfaces*, 2021, **13**, 31298–31309.
12 H. Yu, M. Wu, G. Duan and X. Gong, *Nanoscale*, 2022, **14**, 1296–1309.
13 I. S. Bayer, *Coatings*, 2017, **7**, 12.
14 M. J. Kreder, J. Alvarenga, P. Kim and J. Aizenberg, *Nat. Rev. Mater.*, 2016, **1**, 15003.
15 L. B. Boinovich, A. G. Domantovskii, A. M. Emelyanenko, A. B. Miller, Y. F. Potapov and A. N. Khodan, *Russ. Chem. Bull.*, 2013, **62**, 380–387.
16 V. Zorba, E. Stratakis, M. Barberoglou, E. Spanakis, P. Tzanetakis, S. H. Anastasiadis and C. Fotakis, *Adv. Mater.*, 2008, **20**, 4049–4054.
17 B. Bhushan, Y. C. Jung and K. Koch, *Philos. Trans. R. Soc., A*, 2009, **367**, 1631–1672.
18 M. K. Dawood, H. Zheng, T. H. Liew, K. C. Leong, Y. L. Foo, R. Rajagopalan, S. A. Khan and W. K. Choi, *Langmuir*, 2011, **27**, 4126–4133.
19 R. D. Mukhopadhyay, B. Vedhanarayanan and A. Ajayaghosh, *Angew. Chem., Int. Ed.*, 2017, **56**, 16018–16022.
20 W. Barthlott and C. Neinhuis, *Planta*, 1997, **202**, 1–8.
21 B. Bhushan and Y. C. Jung, *Nanotechnology*, 2006, **17**, 2758–2772.
22 K. Koch and W. Barthlott, *Philos. Trans.: Math., Phys. Eng. Sci.*, 2009, **367**, 1487–1509.
23 K. Koch, B. Bhushan and W. Barthlott, *Soft Matter*, 2008, **4**, 1943–1963.
24 Z. Guo and W. Liu, *Plant Sci.*, 2007, **172**, 1103–1112.
25 S. H. Nguyen, H. K. Webb, P. J. Mahon, R. J. Crawford and E. P. Ivanova, *Molecules*, 2014, **19**, 13614–13630.
26 K. M. Wisdom, J. A. Watson, X. Qu, F. Liu, G. S. Watson and C.-H. Chen, *Proc. Natl. Acad. Sci. U. S. A.*, 2013, **110**, 7992–7997.
27 T. B. H. Schroeder, J. Houghtaling, B. D. Wilts and M. Mayer, *Adv. Mater.*, 2018, **30**, 1705322.
28 J. Genzer and K. Efimenko, *Biofouling*, 2006, **22**, 339–360.
29 N. J. Shirtcliffe, G. McHale, S. Atherton and M. I. Newton, *Adv. Colloid Interface Sci.*, 2010, **161**, 124–138.
30 E. Stratakis, A. Mateescu, M. Barberoglou, M. Vamvakaki, C. Fotakis and S. H. Anastasiadis, *Chem. Commun.*, 2010, **46**, 4136–4138.
31 M. A. Frysali, L. Papoutsakis, G. Kenanakis and S. H. Anastasiadis, *J. Phys. Chem. C*, 2015, **119**, 25401–25407.
32 M. A. Frysali and S. H. Anastasiadis, *Langmuir*, 2017, **33**, 9106–9114.
33 S. Rasouli, N. Rezaei, H. Hamedi, S. Zendehboudi and X. Duan, *Mater. Des.*, 2021, **204**, 109599.
34 W. Zhang, D. Wang, Z. Sun, J. Song and X. Deng, *Chem. Soc. Rev.*, 2021, **50**, 4031–4061.
35 J. Jeevahan, M. Chandrasekaran, G. B. Joseph, R. B. Durairaj and G. Mageshwaran, *J. Coat. Technol. Res.*, 2018, **15**, 231–250.
36 K.-C. Chang, H.-I. Lu, C.-W. Peng, M.-C. Lai, S.-C. Hsu, M.-H. Hsu, Y.-K. Tsai, C.-H. Chang, W.-I. Hung, Y. Wei and J.-M. Yeh, *ACS Appl. Mater. Interfaces*, 2013, **5**, 1460–1467.
37 Y. Wang, Y. Shi, L. Pan, M. Yang, L. Peng, S. Zong, Y. Shi and G. Yu, *Nano Lett.*, 2014, **14**, 4803–4809.
38 L. Dong, Z. Zhang, R. Ding, L. Wang, M. Liu, Z. Weng, Z. Wang and D. Li, *Surf. Coat. Technol.*, 2019, **372**, 434–441.
39 J. Feng, M. T. Tuominen and J. P. Rothstein, *Adv. Funct. Mater.*, 2011, **21**, 3715–3722.
40 R. Fürstner, W. Barthlott, C. Neinhuis and P. Walzel, *Langmuir*, 2005, **21**, 956–961.
41 X. Zhang, J. Zhang, Z. Ren, X. Li, X. Zhang, D. Zhu, T. Wang, T. Tian and B. Yang, *Langmuir*, 2009, **25**, 7375–7382.
42 P. Roach, N. J. Shirtcliffe and M. I. Newton, *Soft Matter*, 2008, **4**, 224–240.
43 F. Gojda, M. Loulakis, L. Papoutsakis, S. Tzortzakis, K. Chrissopoulou and S. H. Anastasiadis, *Langmuir*, 2022, **38**, 4826–4838.
44 J. Ou, W. Hu, M. Xue, F. Wang and W. Li, *ACS Appl. Mater. Interfaces*, 2013, **5**, 3101–3107.
45 C.-H. Xue, Y.-R. Li, P. Zhang, J.-Z. Ma and S.-T. Jia, *ACS Appl. Mater. Interfaces*, 2014, **6**, 10153–10161.
46 W. Hou, Y. Shen, J. Tao, Y. Xu, J. Jiang, H. Chen and Z. Jia, *Colloids Surf., A*, 2020, **586**, 124180.
47 Y. Tuo, H. Zhang, W. Rong, S. Jiang, W. Chen and X. Liu, *Langmuir*, 2019, **35**, 11016–11022.
48 B. K. Nandi, R. Uppaluri and M. K. Purkait, *J. Membr. Sci.*, 2009, **330**, 246–258.
49 J. Zhang, B. Li, L. Wu and A. Wang, *Chem. Commun.*, 2013, **49**, 11509–11511.
50 T. C. Rangel, A. F. Michels, F. Horowitz and D. E. Weibel, *Langmuir*, 2015, **31**, 3465–3472.
51 Y.-S. Cho, S. Nam, S. Jeong and Y.-S. Kim, *J. Dispersion Sci. Technol.*, 2020, **41**, 1526–1539.
52 C. Q. Li, Y. L. Zhan, S. Lei and W. Li, *Int. J. Mater. Res.*, 2019, **110**, 1135–1141.
53 S. A. Mahadik, F. Pedraza and S. S. Mahadik, *Prog. Org. Coat.*, 2017, **104**, 217–222.
54 Z. Lian, J. Xu, P. Yu, Z. Yu, Z. Wang and H. Yu, *Met. Mater. Interfaces*, 2020, **26**, 1603–1610.

55 Y.-Q. Liu, Y.-L. Zhang, X.-Y. Fu and H.-B. Sun, *ACS Appl. Mater. Interfaces*, 2015, **7**, 20930–20936.
56 M. Qu, L. Ma, Y. Zhou, Y. Zhao, J. Wang, Y. Zhang, X. Zhu, X. Liu and J. He, *ACS Appl. Nano Mater.*, 2018, **9**, 5197–5209.
57 J. Yong, F. Chen, Q. Yang, D. Zhang, U. Farooq, G. Du and X. Hou, *J. Mater. Chem. A*, 2014, **2**, 8790–8795.
58 S. Nishimoto and B. Bhushan, *RSC Adv.*, 2013, **3**, 671–690.
59 N. Gao and Y. Yan, *Nanoscale*, 2012, **4**, 2202–2218.
60 Y. Wu, S. Jia, Y. Qing, S. Luo and M. Liu, *J. Mater. Chem. A*, 2016, **4**, 14111–14121.
61 X. Li, B. Li, Y. Li and J. Sun, *Chem. Eng. J.*, 2021, **404**, 126504.
62 L. Gao, Y. Lu, J. Li and Q. Sun, *Holzforschung*, 2016, **70**, 63–68.
63 R. B. Jeen Robert, G. S. Hikku, K. Jeyasubramanian, J. Jacobjose and R. Malkiya Rasalin Prince, *Mater. Res. Express*, 2019, **6**, 75705.
64 G. D. Patil, A. H. Patil, S. A. Jadhav, C. R. Patil and P. S. Patil, *Mater. Lett.*, 2019, **255**, 126562.
65 M. Raeisi, Y. Kazerouni, A. Mohammadi, M. Hashemi, I. Hejazi, J. Seyfi, H. A. Khonakdar and S. M. Davachi, *Int. J. Biol. Macromol.*, 2021, **171**, 158–165.
66 M. Z. Khan, V. Baheti, M. Ashraf, T. Hussain, A. Ali, A. Javid and A. Rehman, *Fibers Polym.*, 2018, **19**, 1647–1654.
67 H. Ogihara, J. Xie, J. Okagaki and T. Saji, *Langmuir*, 2012, **28**, 4605–4608.
68 P. N. Manoudis, A. Tsakalof, I. Karapanagiotis, I. Zuburtikudis and C. Panayiotou, *Surf. Coat. Technol.*, 2009, **203**, 1322–1328.
69 I. Boticas, D. Dias, D. Ferreira, P. Magalhães, R. Silva and R. Fangueiro, *SN Appl. Sci.*, 2019, **1**, 1376.
70 Z. Mai, Z. Xiong, X. Shu, X. Liu, H. Zhang, X. Yin, Y. Zhou, M. Liu, M. Zhang, W. Xu and D. Chen, *Carbohydr. Polym.*, 2018, **199**, 516–525.
71 M. Shaban, F. Mohamed and S. Abdallah, *Sci. Rep.*, 2018, **8**, 3925.
72 M. M. Rashid, B. Simončič and B. Tomšič, *Surf. Interfaces*, 2021, **22**, 100890.
73 C.-H. Xue, S.-T. Jia, H.-Z. Chen and M. Wang, *Sci. Technol. Adv. Mater.*, 2008, **9**, 35001.
74 Y. Kameya and H. Yabe, *Coatings*, 2019, **9**, 547.
75 L. Yang, S. Bai, D. Zhu, Z. Yang, M. Zhang, Z. Zhang, E. Chen and W. Cao, *J. Phys. Chem. C*, 2007, **111**, 431–434.
76 C. H. Han and B. G. Min, *Fibers Polym.*, 2020, **21**, 785–791.
77 B. Zhang, W. Xu, Q. Zhu and B. Hou, *J. Mater. Sci. Technol.*, 2021, **66**, 74–81.
78 X. Zhang, Y. Guo, Z. Zhang and P. Zhang, *Appl. Surf. Sci.*, 2012, **258**, 7907–7911.
79 X. Yu, X. Liu, X. Shi, Z. Zhang, H. Wang and L. Feng, *Ceram. Int.*, 2019, **45**, 15741–15744.
80 D. Aslanidou, I. Karapanagiotis and C. Panayiotou, *Prog. Org. Coat.*, 2016, **97**, 44–52.
81 J.-D. Brassard, D. K. Sarkar and J. Perron, *Appl. Sci.*, 2012, **2**, 453–464.
82 Y. Guo, D. Jiang, X. Zhang, Z. Zhang and Q. Wang, *Appl. Surf. Sci.*, 2010, **256**, 7088–7090.
83 W. Li, X. Tan, J. Zhu, P. Xiang, T. Xiao, L. Tian, A. Yang, M. Wang and X. Chen, *Mater. Today Energy*, 2019, **12**, 348–355.
84 A. Bake, N. Merah, A. Matin, M. Gondal, T. Qahtan and N. Abu-Dheir, *Prog. Org. Coat.*, 2018, **122**, 170–179.
85 H. Papananou, E. Perivolari, K. Chrissopoulou and S. H. Anastasiadis, *Polymer*, 2018, **157**, 111–121.
86 M. Parizek, N. S. Kasalkova, Z. Svindrych, P. Slepicka, M. Bacakova, V. Lisa and V. Svorcik, *BioMed Res. Int.*, 2013, **2013**, 371430.
87 K. Chrissopoulou, I. Altintzi, S. H. Anastasiadis, E. P. Giannelis, M. Pitsikalis, N. Hadjichristidis and N. Theophilou, *Polymer*, 2005, **46**, 12440–12451.